HHS Public Access

Author manuscript

J Genet Genomics. Author manuscript; available in PMC 2021 April 20.

Published in final edited form as:

J Genet Genomics. 2020 April 20; 47(4): 187–199. doi:10.1016/j.jgg.2020.02.008.

Drosophila P75 safeguards oogenesis by preventing H3K9me2 spreading

Kun Dou[a,b,*], **Yanchao Liu**[c,1], **Yingpei Zhang**[c,1], **Chenhui Wang**[a], **Ying Huang**[c,d,*], **ZZ Zhao Zhang**[a,e,f,*]

[a]Department of Embryology, Carnegie Institution for Science, Baltimore, MD, 21218, USA

[b]Current address: School of Life Science and Technology, ShanghaiTech University, Shanghai 201210, China

[c]State Key Laboratory of Molecular Biology, Shanghai Key Laboratory of Molecular Andrology, Shanghai Institute of Biochemistry and Cell Biology, Chinese Academy of Sciences, Shanghai 200031, China

[d]Shanghai Key Laboratory of Biliary Tract Disease Research, Shanghai Research Center of Biliary Tract Disease, Department of General Surgery, Xinhua Hospital, affiliated to Shanghai Jiao Tong University School of Medicine, Shanghai, China, 200092

[e]Department of Pharmacology and Cancer Biology, Duke University School of Medicine, Durham, NC, 27710

[f]Regeneration Next, Duke University, Durham, NC, 27710

Abstract

Serving as a host factor for HIV integration, LEDGF/p75 has been under extensive study as a potential target for therapy. However, as a highly conserved protein, its physiological function remains to be thoroughly elucidated. Here we characterize the molecular function of dP75, the *Drosophila* homolog of LEDGF/p75, during oogenesis. dP75 binds to transcriptionally active chromatin with its PWWP domain. The C-terminus IBD domain-containing region of dP75 physically interacts with the histone kinase Jil-1 and stabilizes it *in vivo*. Together with Jil-1, dP75 prevents the spreading of the heterochromatin mark–H3K9me2–onto genes required for oogenesis

[*]Correspondence: doukun@shanghaitech.edu.cn, huangying@xinhuamed.com.cn, z.z@duke.edu.
[1]These authors contributed equally in this work.

Credit Author Statement

Kun Dou: Conceptualization; Investigation; Methodology; Validation; Data Curation; Formal analysis; Writing-original draft; Writing-review & editing.
Yanchao Liu: Investigation; Methodology; Validation.
Yingpei Zhang: Investigation; Methodology; Validation.
Chenhui Wang: Investigation; Methodology; Validation.
Ying Huang: Supervision; Funding acquisition; Project administration; Validation; Methodology; Writing-original draft; Writing-review & editing.
ZZ Zhao Zhang: Conceptualization; Supervision; Funding acquisition; Project administration; Writing-original draft; Writing-review & editing.

and piRNA production. Without dP75, ectopically silencing of these genes disrupts oogenesis, activates transposons, and causes animal sterility. We propose that dP75, the homolog of an HIV host factor in *Drosophila*, partners with and stabilizes Jil-1 to ensure gene expression during oogenesis by preventing ectopic heterochromatin spreading.

Keywords

Drosophila; LEDGF/p75; Jil-1; H3K9me2

1. INTRODUCTION

P75, also known as PC4 and SFRS1 Interacting Protein 1 (PSIP1) or Lens Epithelium-Derived Growth Factor (LEDGF), is identified as a host factor that recruits the integrase of human immunodeficiency virus-1 (HIV-1) to targeted genomic sites (Cherepanov et al., 2003; Ferris et al., 2010; Gijsbers et al., 2010). Current model suggests that both the PWWP domain (the domain around 70 amino acids with a core 'Pro-Trp-Trp-Pro') and the integrase-binding domain (IBD) from LEDGF/p75 are essential for tethering HIV cDNA to chromatin. While the PWWP domain finds its binding regions on host chromatin (Llano et al., 2006; Shun et al., 2008; Turlure et al., 2006), the IBD from the C-terminus region recruits HIV integrase via physical interaction (Cherepanov et al., 2004; Vanegas et al., 2005). Given its importance for HIV replication, LEDGF/p75 has been intensively studied for drug discovery.

Besides mediating HIV integration, the conservation of LEDGF/p75 across species suggests that it possesses essential molecular functions under physiological condition. In fact, depletion of LEDGF/p75 in mice results in perinatal mortality, and the few ones survived into adulthood show various phenotypic abnormalities, including skeletal defects and decreased fertility (Sutherland et al., 2006). Although LEDGF/p75 appears to be an important factor for animal development, the molecular function of it or its homolog is still largely unknown.

Jil-1 is an interphase H3S10 kinase, which belongs to the serine/threonine tandem kinase family and localizes to chromatin throughout the cell cycle (Wang et al., 2001). It is functionally and structurally conserved from *Drosophila* to mammals (Jin et al., 1999; Wang et al., 2001; Zhang et al., 2003). The N-terminus of Jil-1 harbors a nuclear localization signal, followed by the tandem kinase domains in the middle. The acidic and basic domains at the C-terminus are responsible for targeting Jil-1 correctly to chromatin regions (Li et al., 2013). Disrupting the function of Jil-1 leads to epigenetic changes of its targeting loci, and results in severe developmental defects, including reduced viability, segment specification defect, and female sterility in fruit flies (Zhang et al., 2003). Despite its importance for animal development, the regulators and partners of Jil-1, which may function together with it to maintain the chromatin status, are still to be identified.

Here we identify the *Drosophila* homolog of LEDGF/p75–CG7946, which we refer to as *Drosophila* p75 (dP75). We show that dP75 functions as an important factor to stabilize Jil-1 and ensure normal oogenesis. dP75 uses its PWWP domain to associate with chromatin, and

its C-terminus IBD-containing region to directly interact with and stabilize Jil-1. The dP75-Jil-1 complex protects its targeting loci from deposition of the H3K9me2, an epigenetic modification that typically leads to gene silencing (Cai et al., 2014; Deng et al., 2007; Yasuhara and Wakimoto, 2008). Accordingly, loss of either dP75 or Jil-1 leads to transcriptional suppression of their protected genes, whose expression is essential for safeguarding oogenesis and transposon silencing. Our findings provide mechanistic insights into the physiological function of the LEDGF/p75 homolog during oogenesis.

2. RESULTS

2.1. *CG7946*, the *Drosophila* homolog of LEDGF/p75, is essential for female fertility

With an initial purpose to identify transcriptional regulators of transposons, we surveyed the RNAi alleles of thirty-six genes with putative chromatin binding domains in *Drosophila*. Based on the observation that transposon activation usually leads to female infertility, we tested the female fertility for depletion of each of the thirty-six genes, and found that germline depletion of *CG7946* leads to complete sterility of female flies. BLAST search of CG7946 with human genome suggested that it has high homology with the human LEDGF/p75 protein, which is an intriguing protein with its physiological function to be fully elucidated. Therefore, we decided to focus on how it functions in fly ovary and leads to sterility.

Since *CG7946* is the single candidate in *Drosophila* with high homology with LEDGF/p75, we named it as *dP75* (*Drosophila* p75). Sequence alignment revealed homology for both the PWWP and IBD domains (Fig. 1A, with 63% and 47% positives, respectively). In order to investigate its function, we generated two mutant alleles of *dP75* using CRISPR/Cas9 system with two different sgRNAs (Fig. S1A). The $dP75^{sg1}$ allele lacks the ATG start codon; and the $dP75^{sg2}$ allele has a reading-frame shift from the 66th amino acid, resulting in a premature stop codon at the 91st amino acid (Fig. S1A). To validate that both alleles are strong mutants, we generated a polyclonal antibody against the full-length dP75 protein. While we detected a strong band corresponding to the predicted size of dP75 from the control flies based on western blot, the signal was absent from $dP75^{sg1/sg2}$ flies (Fig. 1B). Immunostaining of dP75 on fly ovaries showed nucleus-localized signals in both germ cells and somatic follicle cells. These signals were undetectable in $dP75^{sg1/sg2}$ mutants (Fig. 1B). These data suggest that neither mutant could produce functional proteins, and thus likely serve as null alleles. To avoid any effects from the potential secondary mutations resulting from CRISPR off-targeting, we used trans-heterozygotes, $dP75^{sg1/sg2}$, in our study and hereafter refer to them as *dP75* mutants.

Loss of dP75 led to female sterility (Fig. 1C). Additionally, reintroducing dP75 into mutants through a transgene fully rescued the fertility defects (Fig. 1C), arguing that dP75 serves as a bona fide factor to maintain female fertility. Next, we sought to determine whether the sterility phenotype of *dP75* is caused by its loss of function in germ cells or somatic follicle cells. To achieve this, we employed cell-type specific RNAi assays (Fig. S1B-S1E). While only depleting dP75 in follicle cells had a marginal effect on fertility, specifically suppressing dP75 in germ cells by RNAi recapitulated the sterility phenotype from the

mutants (Figs. 1D and S1E). Our data thus suggest that dP75 is indispensable in germ cells to maintain fertile oogenesis.

2.2. dP75 binds to actively transcribed genomic regions in fly ovaries

Since the PWWP domain is often involved in chromatin binding (Qin and Min, 2014), we next tested whether dP75 binds to any specific genomic regions in fly ovaries. To facilitate this study, we generated a fly allele that harbors one V5 tag sequence at the endogenous *dP75* locus, thus producing V5::dP75 proteins (Fig. 2A and B). Adding V5 tag appears to have no negative effect on dP75 protein function and localization (Fig. 2A). We next performed chromatin immunoprecipitation followed by high-throughput sequencing (ChIP-Seq). Our ChIP-seq data showed that dP75 preferentially binds to genes engaged in active transcription (Fig. 2C and D). In fly ovaries, there were 6985 genes producing transcripts with the FPKM (Fragments Per Kilobase of transcript per Million mapped reads) ≥ 3. Among them, 6575 (94.1%) showed significant enrichment for dP75 binding (Fig. S2A). On the contrary, for the 9706 genes having an FPKM value lower than 3 in fly ovaries, only 2092 (21.5%) of them were enriched with dP75 binding (Fig. S2A). Additionally, we calculated the enrichment of dP75 peaks over intergenic regions, 5' and 3'UTRs, and exonic and intronic regions respectively. While intergenic regions had minimum, if any, binding of dP75, it showed strong enrichment over exons and the 5′ and 3′ UTRs (Fig. S2B).

To explore how dP75 is recruited to its targeting loci on chromatin, we employed Isothermal titration calorimetry (ITC) to measure the binding affinity of purified PWWP domain to a few potential substrates: single-stranded DNA, double-stranded DNA, peptides of H3K4me3, H3K9me3, H3K27me3, and H3K36me3. The PWWP domain of dP75 had high binding affinity with double-stranded DNA (K_D = 3.6±2.9 μM) and Oligo-dT single-stranded DNA (K_D = 4.8±0.7 μM) (Fig. 2E). When using different modified histone peptides as substrates, it did not exhibit any binding preference with them except for a low affinity with H3K36me3 (K_D > 500 μM, Fig. 2E), a histone marker for transcriptionally active genes (Kolasinska-Zwierz et al., 2009). Our *in vitro* data suggest that dP75 is recruited to chromatin by H3K36me3 and this binding might be further enhanced by interacting with DNA.

2.3. dP75 physically interacts with histone kinase Jil-1 both *in vivo* and *in vitro*

Given that the IBD (Integrase Binding Domain) of mammalian p75 often mediates protein interactions (Tesina et al., 2015), we performed V5 IP-mass spectrometry to search for the binding partners of dP75 in V5::dP75 fly ovaries. From the V5::dP75 ovary lysate, we recovered 149 peptides from dP75, which was listed as the top hit from mass spectrometry data. In control lysates derived from the flies without a V5 tag, we did not detect any peptides derived from dP75, highlighting the high stringency of our IP condition (Fig. 3A). Besides dP75, the second strongest hit was from histone kinase Jil-1 in V5::dP75 lysate (with 14 peptides being detected), but none from the control (Fig. 3A). Supporting our findings, a previous study in *Drosophila* S2 cells also captured Jil-1 and CG7946/dP75 in the same complex (Wang et al., 2013). Accordingly, we also noticed that Jil-1 and dP75 colocalize in the nucleus of both germ cells and somatic follicle cells in fly ovaries (Fig. 3B).

We next tested whether the interaction between dP75 and Jil-1 is direct. To do this, we used a yeast two-hybrid assay (Y2H) with the beta-galactosidase activity as a readout. Full-length dP75 showed interaction with either the full-length Jil-1 or the C-terminal fragment of Jil-1 (residues 984–1122), but not the N-terminal domain or the kinase domain (Fig. 3C). We then sub-divided dP75 and tested the interaction between each fragment and the C-terminus region of Jil-1 to further map the interaction region on dP75 by Y2H. The C-terminus fragment including the IBD of dP75 was shown to be responsible for binding with Jil-1 (Fig. S3).

Human LEDGF/P75 has been reported to interact with its cellular binding partners via a conserved (E/D)-X-E-X-F-X-G-F motif on these proteins (Tesina et al., 2015). Two regions containing the FYGF sequence are found within the C-terminal fragment of Jil-1, which are located at the proximal site (residue 989–992) and the distal site (residues 1107–1110), respectively. To validate the interactions between dP75 and Jil-1, we performed isothermal titration calorimetry (ITC) using different Jil-1 peptides. The binding to the peptide from the proximal site (EVQADFYGFDE; residues 984–1004) is 150-fold stronger (K_D = 0.8 ± 0.1 μM) than to the peptide at the distal site (KREENFYGFSK; residues 1102–1112; K_D = 120.5 ± 14.5 μM). Alanine substitution of the key residues (F989A, G991V, and F992A) dramatically reduced the binding (Fig. 3D). Taken together, our data indicate that in fly ovaries, dP75 uses its IBD-containing C-terminus region to recruit the histone kinase Jil-1 by directly interacting with its Cterminus (Fig. 3E).

2.4. dP75 is required to stabilize Jil-1 protein *in vivo*

Since dP75 possesses chromatin binding property and physically interacts with Jil-1, we next tested whether Jil-1 localization is dP75 dependent. Either depleting or mutating dP75 resulted in a dramatic reduction of the endogenous Jil-1 in the nucleus (Figs. 4A and S4A). To further validate this dependency, we next generated mosaic ovaries containing *dP75* mutant cells in adjacent to dP75 heterozygotes or wild-type cells within the same ovariole (Fig. 4B). This ensures all cells were treated and imaged under identical conditions. As shown in Fig. 4C, Jil-1 staining gave rise to nuclear foci in the cells producing dP75 (marked by the presence of GFP). In contrast, *dP75* mutant cells always displayed very weak, if any, Jil-1 signals (Fig. 4C). To validate this result, we introduced Flag::Myc tagged Jil-1 transgene under a germline specific driver to either wild-type or ovaries with dP75 depleted in germ cells, and performed both immunostaining and western blot to detect the expression of transgenic Jil-1 protein. Results from both experiments showed that without dP75, the levels of transgenic Jil-1 reduced to nearly undetectable (Fig. 4D and E). Because loss of dP75 (either by RNAi depletion or mutation) had no influence on the steady state level of Jil-1 mRNA (Figs. 4F and S4B), these results indicate that dP75 is required to stabilize Jil-1 protein *in vivo*. On the contrary, dP75 abundance does not depend on Jil-1 (unpublished data).

2.5. dP75 antagonizes ectopic H3K9me2 spreading

Previous studies suggested that Jil-1 is responsible for interphase H3S10 phosphorylation and antagonizes the H3K9me2 in salivary glands (Deng et al., 2007; Zhang et al., 2006). However, interphase H3S10 phosphorylation in nurse cells is below the detection threshold,

and only dividing follicle cells were labeled by antibody staining (unpublished data). We next investigated whether dP75 is responsible for antagonizing H3K9me2 during oogenesis. In wildtype fly ovaries, immunostaining of H3K9me2 showed limited bright puncta in the nucleus (Fig. 5A). Loss of dP75 appears to lead to broader deposition of H3K9me2 in ovarian cells (Fig. 5A), suggesting the spreading of H3K9me2. To test whether dP75 indeed inhibits H3K9me2 spreading with base-pair resolution, we performed ChIP-seq experiments. In wild-type fly ovaries, we detected strong enrichment of H3K9me2 modification at the pericentromeric regions, consistent with previous findings (Yasuhara and Wakimoto, 2008). However, in *dP75* mutant ovaries, the intensity of H3K9me2 peaks decreased at the pericentromeric regions, while we detected more even deposition across chromosome arms (Fig. 5B).

Given that H3K9me2 deposition often promotes gene silencing (Caro et al., 2012), we next performed mRNA sequencing (RNA-Seq) to determine whether loss of dP75 affects gene expression. In *dP75* mutant ovaries, we detected 74 genes that decreased their mRNA abundance by more than 3-fold (Fig. 5C). Among them, 37 also showed > 3-fold reduction upon depleting dP75 specifically in germ cells (Fig. 6A). Closer examination of the top decreased genes on the genome-browser revealed that in wild-type fly ovaries, dP75 binding antagonizes the deposition of H3K9me2 onto them (Fig. 5D). Upon loss of dP75, they were coated by H3K9me2, and were ectopically repressed at the transcriptional level (Fig. 5D).

2.6. dP75 and Jil-1 function together to ensure oogenesis

Given the interactions between dP75 and Jil-1, we next asked whether Jil-1 has similar impacts on oogenesis. Depleting Jil-1 in germline cells also led to the spreading of H3K9me2 on chromosomes (Fig. S5A–C). Additionally, our transcriptome analysis revealed that the same group of genes was suppressed upon loss of Jil-1 or dP75 (Fig. 6A and B). Without Jil-1 being produced in ovarian germ cells, we detected 13 genes significantly decreased for > 5-fold at mRNA level (Fig. 6A). Among them, 12 were also repressed when dP75 was absent (Figs. 5C and 6A). Similar to dP75, Jil-1 from the germline cells is essential for the maintenance of animal fertility (Fig. S5D).

Phenotypically, depleting dP75 or Jil-1 in germ cells resulted in similar oogenesis defects: irregular sized egg chambers along the ovariole; more than 15 nurse cells encapsulated in one egg chamber; five-blob nurse cell chromosome structure in late stage egg chambers (Fig. 6C and Table S1), suggesting that these nurse cells failed to pass the five-blob configuration. Each blob in the five-blob structure represents one major polytenic chromosomal arm, and the five-blob structure are normally observed in the nucleus of nurse cells during stages 4–5 of oogenesis (Klusza and Deng, 2010). The observation of smaller nurse cells with five-blob structure in late stage egg chambers suggests impaired endocycle of these cells. It should be noted that upon dP75 depletion in germ cells, the ovary overall is able to complete oogenesis stages during the time window we investigated (4–8-day-old flies), as indicated by the generally normal morphology and slightly smaller size of these ovaries (Fig. S1D), and the fact that they are able to produce eggs, though with the total amount less than wild type. Moreover, we also observed severe oocyte karyosome defects when dP75 or Jil-1 was absent from germ cells. During oogenesis, oocyte chromosomes arrested at the meiosis prophase I

stage were packaged into a subnuclear structure named karyosome, appearing as a condensed round structure (Staeva-Vieira et al., 2003). In control ovaries, almost all of the stage 7–8 egg chambers had normal karyosome (98%, $n = 56$). However, loss of dP75 in germ cells resulted in 27% of oocytes in these stages having stretched karyosome ($n = 55$; Fig. 6C). The defective karyosomes were also frequently observed in ovaries upon Jil-1 depletion (34% of stage 7–8 egg chambers, $n = 92$; Fig. 6C). All the above results indicate that dP75 and Jil-1 function together to maintain fertile oogenesis.

2.7. dP75 is required for transposon silencing

From our RNA-Seq data, we noticed that BoYb, a piRNA component (Handler et al., 2011), is among the top targets protected by dP75 and Jil-1 (Figs. 7A and S6A). Its mRNA decreased 95% and 80%, respectively, upon dP75 or Jil-1 depletion in fly ovaries (FPKM: 28.78 in control ovaries, 1.58 in dP75 depleted ovaries, and 5.74 in Jil-1 depleted ovaries). Consistently, CG7946/dP75 was previously recovered in a genome-wide screen identifying piRNA pathway components globally (Czech et al., 2013). Given the importance of BoYb in transposon silencing in germ cells (Handler et al., 2011), we measured transposon transcripts in fly ovaries when dP75 is absent. Our RNA-Seq experiments showed that 21 transposon families increased their transcripts by more than 2-fold in *dP75* mutants (Fig. 7B). The elevation of transposon mRNA was further validated by RNA FISH (Fig 7C). Consistently, transposon transcripts also increased upon loss of Jil-1 in germ cells (Fig. S6B), including Burdock and HMS-Beagle, which were the most affected transposon families in *dP75* mutants. Taken together, our data indicate that the dP75-Jil-1 complex is essential for transposon suppression during oogenesis, likely by promoting the expression of key piRNA pathway components, such as BoYb (Fig. 7D). Consistent with this, germline depletion of BoYb also leads to female sterility (unpublished data).

3. DISCUSSION

By studying the physiological function of the homolog of mammalian p75 (dP75), here we uncover its molecular role on ensuring fruit fly oogenesis. Our study reveals that dP75 binds to actively transcribed chromatin via its PWWP domain. Through the IBD-containing C-terminus region, it recruits Jil-1, a histone kinase for the phosphorylation of the 10^{th} residue of Histone 3 (H3S10) (Wang et al., 2001; Zhang et al., 2006), and stabilizes Jil-1 *in vivo*. Previous findings suggest that H3S10 phosphorylation antagonizes the methylation of H3K9, and thus counteracting gene silencing (Zhang et al., 2006; Bao et al., 2007). Consistently, dP75-Jil-1 binding appears to block the spreading of H3K9me2, thus promoting the expression the genes that are essential for oogenesis and transposon silencing (Fig. 7D).

In humans, LEDGF/p75 interacts with chromatin regions that are actively transcribing (De Rijck et al., 2010), thus facilitating HIV integration into these loci (Ferris et al., 2010; Vanegas et al., 2005). Human LEDGF/p75 harbors one PWWP domain and two AT-hooks, all of which appear to contribute to target binding (Llano et al., 2006). The PWWP domain of human LEDGF/p75 shows binding affinity to mononucleosomes with trimethylated Histone 3 at lysine 36 (H3K36me3) *in vitro* (Eidahl et al., 2013), which usually marks

actively transcribed regions (Bannister et al., 2005; Barski et al., 2007). As its name indicates, the two AT-hooks can directly bind to the minor groove of adenine-thymine (AT) enriched DNA (Llano et al., 2006; Reeves and Nissen, 1990). Therefore, with the PWWP domain and AT hooks functioning cooperatively, human LEDGF/p75 can simultaneously interact with both modified histones and DNA from transcribing regions.

We find that during oogenesis, the transcribing loci from the fly genome are also covered by dP75, but likely via a distinct molecular mechanism. While still maintained the PWWP domain, dP75 lacks the AT hooks. However, it appears that its PWWP domain has binding affinity to both modified histones and DNA. When using H3K36me3 peptide as substrate, we detected weak but selective binding. Interestingly, although without the AT-hooks, our *in vitro* data indicate that the PWWP domain from dP75 can still recognize DNA, especially dT, revealing a new binding mode for this domain. It is worth noting that the 3'-untranslated regions from the *Drosophila* genome have a higher AT content, compared with coding regions (Zhang et al., 2004). And we indeed observed that dP75 has a higher affinity towards the 3'UTR regions. Thus, unlike its mammalian homolog which uses the PWWP and AT hooks coordinately to bind chromatin, the PWWP domain itself may facilitate the recruitment of dP75 to both modified histone and DNA simultaneously, resulting in the selection of targeting regions.

Via its C-terminus IBD-containing domain, dP75 stabilizes and recruits a putative interphase histone kinase, Jil-1, to its binding sites. Jil-1 was shown to antagonize the H3K9me2 epigenetic mark in previous study (Zhang et al., 2006; Deng et al., 2007). We found dP75 functions together with Jil-1 to prevent the spreading of H3K9me2, thus likely maintaining local chromatin at an active state to ensure oogenesis. On the contrary, the dP75-Jil-1 complex has mild, if any, effects on the H3K9me3 epigenetic mark (unpublished data). It appears that the dP75 and Jil-1 partnership is not only restricted within ovaries, previous mass spectrometry experiments also captured them in the same complex in S2 cells (Wang et al., 2013), which were likely derived from a macrophage-like lineage. While we were preparing this manuscript, another group independently reported the identification of CG7946/dP75/JASPer (Jil-1 Anchoring and Stabilizing Protein) from *Drosophila* embryo nuclear extracts (Albig et al., 2019). Consistently, we also observed dP75 expression in somatic tissues, albeit at a slightly lower level compared with ovary. Interestingly, in somatic cells, Jil-1 also binds to transcribing regions, subsequently propelling transcription (Regnard et al., 2011). Given that the gene repertoire for active transcription is fundamentally different between germline and somatic tissues, the dP75Jil-1 complex unlikely regulates the same set of targets in different cell types. This indicates that dP75 is recruited at the downstream of transcription initiation, rather than defining gene regions for activation. Thus, we propose that the general function of dP75-Jil-1 complex is protecting transcribing regions from ectopic spreading of H3K9me2, thus fine-tuning gene expression. This predicts that loss of dP75 or Jil-1 would not globally affect gene expression, but might lead to gene suppression when there is a high level of local H3K9me2. Our transcriptome data from dP75 or Jil-1 depleted ovaries indeed support this hypothesis.

Mice with compromised LEDGF/p75 expression suffer with fertility defects (Sutherland et al., 2006), but the underlying molecular mechanism is still unclear. Phylogenetic analysis

shows that the closest mammalian homolog of Jil-1 is MSK1, which is also an H3S10 kinase and has been suggested to fine tune gene expression under stress conditions (Reyskens and Arthur, 2016). Interestingly, both LEDGF/p75 and MSK1 are highly expressed in mouse ovaries (unpublished data). Additionally, previous studies demonstrate that LEDGF/p75 binds with MLL1 complex (Mereau et al., 2013; Yokoyama and Cleary, 2008), and MLL1 is suggested to physically interact with MSK1 (Wiersma et al., 2016). Therefore, the partnership between dP75 and Jil-1 is likely to be conserved in mammals. Perhaps so does their molecular function on safeguarding oogenesis.

4. MATERIALS AND METHODS

The key reagents used in this study are listed in Table 1.

4.2. Fly strains and husbandry conditions

The following fly lines were used: MTD-Gal4: P(otu-Gal4::VP16.R)1 w[*]; P(Gal4-nos.NGT)40; P(Gal4::VP16-nos.UTR)CG6325[MVD1], *mcherry*-sh (attP2) (Bloomington Stock Center), *jil1*-sh (attP2) (Bloomington Stock Center), *dP75*-sh (attP40) (Bloomington Stock Center), $dP75^{sg1}/dP75^{sg2}$ (this study), V5::dP75 (this study), UASp-Flag::Myc::Jil-1 (sttP2, this study), UASp-Flag::Myc::dP75 (attP40, this study). All fly strains were maintained at room temperature on standard agar-corn medium.

4.3. Hatch ratio test

Four to six virgin females of 4–6-day-old with corresponding genotype, as well as equal number of wild type Origen R males were put together in an empty bottle, and molasses plate with a chunk of wet yeast paste on it was served each day to the flies. Molasses plates were collected after 24 hours to allow females to lay eggs on them, and maintained at room temperature for another 24–30 hours to allow eggs to hatch. Hatching rates were calculated by dividing the number of hatched eggs to number of total eggs laid each day. Four to six females were used for each genotype in each test, and at least two independent replicates were performed and reached the same conclusion.

4.4. Generation of knockout and knockin flies with CRISPR/Cas9

For knockout flies, two separate sgRNAs were designed by using the webpage "http://tools.flycrispr.molbio.wisc.edu/targetFinder/index.php". PCR sgDNAs by using pRB17 plasmid and sgRNA core as templates, and using U6_promo_F, sgRNA_U6term_R, and U6_yourguide_F together as primers. Note that sequence of the guide RNA I used was incorporated in the U6_yourguide_F primer. This overlapping PCR generated a single product of around 560 base pair, with U6 promoter followed by sgDNA sequence. The purified PCR products were sent out to Rainbow company for transgenic fly to inject the *y*,vas-Cas9 fly stain. PCR products of sgRNA for *white* were co-injected to the flies. The hatched flies from the injection were mated to balancer flies individually, and the second generation from each individual cross was first sorted based on eye color, followed by examination of whether our target gene *dP75* was disrupted using PCR and sequencing. Negative flies from the injection with the same background but without disruption of *dP75* were used as control animals.

To generate V5::dP75 flies, donor sequence was generated by annealing 800bp left arm homology sequence, V5 tag sequence, and 600bp right arm homology sequence together by Gibson assembling, and cloning into pUC19 plasmid. Note that both PAM sequences corresponding to the two sgRNAs were mutated in the V5 knock-in construct to avoid cutting in the successful knock-in flies. Purified PCR products of two separate sgRNAs (as prepared above) and *white* sgRNA, as well as the donor plasmid were provided for injection of *y*,vas-Cas9 flies. Flies from the injection were sorted similar as described above for the knock-out injection, and followed by PCR and sequencing for the region of *dP75* to ensure knock-in fidelity. All the constructs, sequences, and successful knock-in and knock-out flies were identified by PCR and verified by sequencing corresponding regions.

4.5. Immunostaining

Five pairs of ovaries from 4–8 day old flies were dissected in PBS, and immediately submerged in PBS with 4% formaldehyde for 12 min. Then ovaries were washed in PBST (PBS solution supplemented with 0.2% Triton X-100) for 3 times with a total of 30 min. Ovaries were blocked in PBST with 9% NGS overnight at 4 °C. Primary antibodies were added in blocking buffer after that, and ovaries were incubated for another 12 hours at 4 °C. Ovaries were washed for 3 times with a total of 30 min, and then incubated in blocking buffer with secondary antibody overnight at 4 °C. Ovaries were washed for another 3 times with a total of 30 min, followed by incubation in PBS with DAPI for 8 min. Ovaries were washed twice before mounting with 20 μL Vectashield Mounting Medium. Primary antibodies used in this study include: anti-dP75 (1:100), anti-V5 (1:100), anti-Jil-1 (1:100), anti-H3K9me2 (1:500). At least two independent replicates were performed for each staining and reached the same conclusion.

4.6. Mosaic Analysis

For mosaic analysis, the 82B FRT flies was recombined with *dP75* mutant to generate 82B FRT, *dP75* - / *TM6c, sb* flies. These flies were crossed with hs-FLP; 82B FRT, ubi-GFP flies to generate hs-FLP; 82B FRT, *dP75* - / 82B FRT, ubi-GFP flies. The adult female flies were heat-shocked at 37 °C for 30 min each day for 4–7 days. These females were subjected to immunostaining following the immunostaining protocol above. Two independent batches of flies were collected for heat-shock and immunostaining and reached the same results. At least two independent replicates were performed and reached the same conclusion. Four to six flies were used for each replicate.

4.7. Affinity purification and mass spectrum analysis

Fifty pairs of fly ovaries from V5 knock-in flies at the endogenous *dP75* locus, as well as the same amount of wild type fly ovaries without V5 tag were dissected in cold PBS, and subjected to lysis with HEPES NP40 lysis buffer (50mM HEPES, KOH ph7.5, 150mM KCl, 3.2 mM MgCl2, 0.5% NP40, supplemented with Roche EDTA free complete protease inhibitor right before use). Sonicate the lysate in bioruptor on medium strength for 7 min (15 sec on, 1 minute off). The supernatants were collected after spin at top speed, and subjected to immunoprecipitation. V5 agarose beads of 40 μL were washed in lysis buffer and applied to each sample, followed by incubation of 3–5 hours at 4°C with gentle rotation. After IP,

the beads are washed three times with the lysis buffer, and proteins were eluted with 40 μL lysis buffer supplemented with 150 μg/mL V5 peptide.

The elutions were sent to Mass Spectrometry and Proteomics Facility of Johns Hopkins university for mass spectrum analysis.

4.8. Antibody generation

Full-length dP75 protein with GST tag was purified from BL21 *E.coli* by using Glutathione Sepharose 4B GST-tagged protein purification resin (GE healthcare, 17075601) and following the protocol in GE healthcare webpage. The purified protein was sent to Pocono Rabbit Farm for polyclonal antibody production in rabbit. The final bleed showed highest efficiency and was used in western blot and immunostaining experiments.

4.9. ChIP-Seq

Fifty pairs of fly ovaries were dissected in cold PBS for each sample, and fixed by paraformaldehyde at a final concentration of 1.8% for 10 min. Glycine was added to a final concentration of 125mM to stop fixation. The samples were washed with cold PBS and immersed in sonication buffer (50mM Tris-HCl pH8.0, 10mM EDTA, 1% SDS). Protease inhibitor was added right before use). Samples were sonicated with bioruptor, followed by spinning at top speed to remove the pellet. The lysates were diluted ten times, and 100 μL diluted lysate was saved as input, and the rest were used for IP. For IP, equal amount (25 μL) of washed protein A and protein G beads were first incubated with antibody for 3–4 hours at 4 °C. Then the lysates were applied to beads, and incubated at 4 °C overnight with gentle rotation. After IP, the beads were washed with low salt, high salt, LiCl buffer, and TE buffer sequentially. Direct elution buffer (10 mM Tris-HCl pH 8.0, 300 mM NaCl, 5 mM EDTA, and 0.5% SDS) was added, and samples were incubated at 65 °C for 6 hours for elution. The eluted DNA was extracted by phenol/chloroform, and was used for library preparation. The libraries were sequenced by Illumina NextSeq with single-end 75nt runs. The ChIP-Seq data were analyzed by piPipes (Han et al., 2015) and deepTools, and the same number of mapped reads was used for comparison between control and experimental groups. Two independent replicates were performed and reached the same conclusion.

4.10. mRNA sequencing

Total RNAs were extracted from six pairs of 4–6 day old fly ovaries of each sample, followed by ribosomal RNA depletion with RiboZero magnetic kit and Turbo DNase treatment. These RNAs were purified by RNA Clean & Concentrator-5 kit. The purified RNAs were subjected to library preparation by following the protocol described (Zhang et al., 2012). Libraries were sequenced with Illumina NextSeq with paired-end 75nt runs. The RNA-Seq data were analyzed by piPipes (Han et al., 2015) and hisat2. FPKM were calculated and used for plots. During plotting process, few genes with FPKM larger than 2^13 are not shown in the plots since none of them showed altered expression by loss of either Jil-1 or dP75. Two independent replicates were performed for each genotype.

4.11. Plasmid construction

For UASP-Flag::Myc::dP75 construct, full length dP75 was amplified from fly cDNA, and cloned to gateway entry vector, followed by recombination to UASP-Flag:Myc gateway destination vector with the attB sites. The positive colonies were validated by sequencing. The UASP-Flag::Myc::Jil-1 was constructed in similar way. For *in vitro* assays, DNA fragment encoding the PWWP domain of dP75 (residues 8–91) was cloned into the pET28-SMT3 vector between the *BamH*I and *Sal*I sites, which contains an N-terminal Ulp1 cleavable His6-SUMO tag. *dP75* plasmid with mutations were generated by Site-Directed Mutagenesis Kit (NEB). For yeast two-hybrid assays, fragments of dP75 (residues 1–475, 1–90, 85–300, 211–475, 209–445, 423–475) were cloned between *BamH*I and *Sal*I sites of the pBTM116 vector (Clontech). Fragments of Jil1 (residues 1–1207, 1–255, 255–541, 525–990, 984–1122, and 1100–1207) were cloned between *BgI*II and *Xho*I sites of the pACT2 vector (Clontech). All the mutants were generated using a Site-Directed Mutagenesis Kit (NEB) according to the manufacturer's instructions. All constructs were sequence verified.

4.12. Protein expression and purification

For *in vitro* assays, His_6-SUMO-tagged recombinant proteins were expressed in *Escherichia coli* BL21 (DE3) under kanamycin selection. Cells were grown to an OD_{600} of 0.6, and protein expression was induced with 0.2 mM IPTG overnight at 18°C. The cells were collected by centrifugation at 4,000 rpm for 15 min and were lysed by French Press (JNBIO) at 4 °C. His6SUMO-tagged proteins were purified by affinity chromatography using a HisTrap HP column (GE Healthcare), followed by the cleavage of the His_6-SUMO tag using Ulp1 protease. The proteins were further purified by ion-exchange chromatography using a HiTrap S column (GE Healthcare) and eluted in a gradient of NaCl. Size-exclusion chromatography was performed for the final purification of wild-type and mutant dP75 PWWP using Superdex G75 Hiload 16/60 column (GE Healthcare). Fractions containing target proteins were pooled and concentrated to 10 mg/ml in a buffer containing 10 mM Tris-HCl, pH 8.0, 100 mM NaCl, and 1 mM DTT.

4.13. Isothermal titration calorimetry (ITC)

DNA fragments used in ITC were synthesized (Sangon). dP75 PWWP as well as DNA fragments or histone peptides were dialyzed overnight in a buffer containing 10 mM Tris, pH 8.0, 100 mM NaCl. ITC measurements were performed in duplicates at 20 °C, using an iTC200 (MicroCal, Inc). The samples were centrifuged before the experiments to remove any precipitates. Experiments were carried out by 20 injections of 2 μL of 2 mM DNA solution into the sample cell containing 0.2 M of dP75 PWWP in the dialysis buffer. Experiments were carried out by 20 injections of 2 μL of 1 mM wild-type or mutant Jil-1 peptides (1102–1112, 984–1004, 984–1004 (WT, F989A, G991V, F992A)) into the sample cell containing 0.1 mM of dP75 IBD-containing C-terminus region (residues 209–445) in the dialysis buffer. Binding isotherms and standard deviation were derived from nonlinear fitting using Origin 8.0 (MicroCal, Inc). The initial data point was routinely deleted. The ITC data were fit to a one-site binding model in 1:1 binding mode.

4.14. Yeast two-hybrid assay

The yeast two-hybrid assays were performed with L40 strains containing pBTM116 and pACT2 fusion plasmids. The colonies containing both plasmids were selected on Leu-Trp- plates. To determine the strength of protein–protein interactions, β-galactosidase solution assays were performed using ortho-nitrophenyl-β-galactopyranoside (ONPG) as the substrate. The cells were inoculated into Leu-Trp-media and grown at 30 °C with vigorous shaking until the OD_{600} reached 0.6–1. At least three independent clones were selected. The cells (2mL) were harvested, centrifuged, and resuspended in 0.1 mL Z buffer (16.1 g/L $Na_2HPO_4{\cdot}7H_2O$, 5.50 g/L $NaH_2PO_4{\cdot}H_2O$, 0.75 g/L KCl, 0.246 g/L $MgSO_4{\cdot}H_2O$, pH 7.0), frozen in liquid nitrogen, and thawed at 37 °C in a water bath. Repeat this step for two more times to lysis cells completely. Then the reaction systems (0.2 mL 4mg/mL ONPG in Z buffer and 0.9 mL 0.27% β-mercaptoethanol in Z buffer per 0.1 mL yeast cell resuspensions) were placed in a 30 °C incubator. After the yellow color developed, 0.5 mL 1 M Na_2CO_3 was added to the reaction and blank tubes. Reaction time was recorded in min. Reaction tubes were centrifuged at 14,000 g for 10 min and supernatants were carefully transferred to clean cuvettes and OD_{420} of the samples relative to the blank was recorded. At last, the β-galactosidase units were calculated using the following formula: β-galactosidase units = $1000\times OD_{420}/(t\times V\times OD_{600})$, where t is the reaction time (in minute) of incubation, V is the volume and in this case V=2, OD_{600} is the cell density of the culture.

4.15. RNA FISH

The RNA FISH experiments were carried out according to the protocol described in Wang et al. (2018). Briefly, Stellaris RNA FISH probes were designed and purchased from LGC Bioresearch Technology. 3–5 pairs of ovaries were dissected in cold PBS, and fixed in 4% formaldehyde for 20 min. Ovaries were washed once with PBST and twice with PBS, followed by immersing in 70% (v/v) ethanol for 8 h at 4 °C. Then ovaries were washed with Wash Buffer A (LGC Biosearch Tech, Cat# SMF-WA1–60) at room temperature for 5 min, and incubated with 50 μL Hybridization Buffer (LGC Biosearch Tech, Cat# SMF- HB1–10) containing RNA probe set overnight at 37 °C. After that, ovaries were washed twice with Wash Buffer A at 37 °C for 30 min and once with Wash Buffer B (LGC Biosearch Tech, Cat# SMF- WB1–20) at room temperature for 5 min. Samples were mounted after final wash. Two independent replicates were performed for each genotype.

4.16. QUANTIFICATION AND STATISTICAL ANALYSIS

The number of animals examined is indicated in Materials and methods. Student's *t* test was carried out, and the results are shown as mean ± standard deviation (SD). The biostatistics of deep-sequencing libraries is listed in Table S2.

4.17. DATA AND SOFTWARE AVAILABILITY

Deep sequencing data are deposited to NCBI (PRJNA589981).

Supplementary Material

Refer to Web version on PubMed Central for supplementary material.

ACKNOWLEDGMENTS

We thank the Johansen lab for providing Jil-1 antibody. We thank members from ZZ lab, Spradling lab, and Bortvin lab for valuable suggestions. We thank Dr. Wanbao Niu for sharing unplublished RNA sequencing data from mouse ovary. We thank Dr. Ethan Greenblatt and Dr. Steven DeLuca for precious advises and discussion on the project. We thank Dr. Allan Spradling and Dr. Robert Levis for proof-reading of the manuscript. We thank Dr. Frederick Tan for trouble shooting in the deep-sequencing analysis. We thank Carnegie Institution for Science, department of Embryology, and ShanghaiTech for instrumental supports. We thank Shanghai Science Research Center and Zhangjiang Laboratory for their instrumental support and technical assistance. This work was supported by the grant from the NIH to Z.Z. (DP5OD021355), as well as the National Natural Science Foundation of China (91940302 and 31870741 to Y.H.).

Abbreviations

LEDGF	Lens Epithelium-Derived Growth Factor
PWWP domain	Pro-Trp-Trp-Pro' domain

REFERENCES

Albig C, Wang C, Dann GP, Wojcik F, Schauer T, Krause S, Maenner S, Cai W, Li Y, Girton J, Muir TW, Johansen J, Johansen KM, Becker PB, Regnard C, 2019 JASPer controls interphase histone H3S10 phosphorylation by chromosomal kinase JIL-1 in Drosophila. Nat. Commun. 10, 5343. [PubMed: 31767855]

Bannister AJ, Schneider R, Myers FA, Thorne AW, Crane-Robinson C, Kouzarides T, 2005 Spatial distribution of di- and tri-methyl lysine 36 of histone H3 at active genes. J. Biol. Chem. 280, 17732–17736. [PubMed: 15760899]

Bao X, Deng H, Johansen J, Girton J, Johansen KM, 2007 Loss-of-function alleles of the JIL-1 histone H3S10 kinase enhance position-effect variegation at pericentric sites in Drosophila heterochromatin. Genetics 176, 1355–1358. [PubMed: 17435241]

Barski A, Cuddapah S, Cui K, Roh TY, Schones DE, Wang Z, Wei G, Chepelev I, Zhao K, 2007 High-resolution profiling of histone methylations in the human genome. Cell 129, 823–837. [PubMed: 17512414]

Cai W, Wang C, Li Y, Yao C, Shen L, Liu S, Bao X, Schnable PS, Girton J, Johansen J, Johansen KM, 2014 Genome-wide analysis of regulation of gene expression and H3K9me2 distribution by JIL-1 kinase mediated histone H3S10 phosphorylation in Drosophila. Nucleic Acids Res. 42, 5456–5467. [PubMed: 24598257]

Caro E, Stroud H, Greenberg MV, Bernatavichute YV, Feng S, Groth M, Vashisht AA, Wohlschlegel J, Jacobsen SE, 2012 The SET-domain protein SUVR5 mediates H3K9me2 deposition and silencing at stimulus response genes in a DNA methylation-independent manner. PLoS Genet. 8, e1002995.

Cherepanov P, Devroe E, Silver PA, Engelman A, 2004 Identification of an evolutionarily conserved domain in human lens epithelium-derived growth factor/transcriptional co-activator p75 (LEDGF/p75) that binds HIV-1 integrase. J. Biol. Chem. 279, 48883–48892. [PubMed: 15371438]

Cherepanov P, Maertens G, Proost P, Devreese B, Van Beeumen J, Engelborghs Y, De Clercq E, Debyser Z, 2003 HIV-1 integrase forms stable tetramers and associates with LEDGF/p75 protein in human cells. J. Biol. Chem. 278, 372–381. [PubMed: 12407101]

Czech B, Preall JB, McGinn J, Hannon GJ, 2013 A transcriptome-wide RNAi screen in the Drosophila ovary reveals factors of the germline piRNA pathway. Mol. Cell 50, 749–761. [PubMed: 23665227]

De Rijck J, Bartholomeeusen K, Ceulemans H, Debyser Z, Gijsbers R, 2010 High-resolution profiling of the LEDGF/p75 chromatin interaction in the ENCODE region. Nucleic Acids Res. 38, 6135–6147. [PubMed: 20484370]

Deng H, Bao X, Zhang W, Girton J, Johansen J, Johansen KM, 2007 Reduced levels of Su(var)3–9 but not Su(var)2–5 (HP1) counteract the effects on chromatin structure and viability in loss-of-function mutants of the JIL-1 histone H3S10 kinase. Genetics 177, 79–87. [PubMed: 17660558]

Eidahl JO, Crowe BL, North JA, McKee CJ, Shkriabai N, Feng L, Plumb M, Graham RL, Gorelick RJ, Hess S, Poirier MG, Foster MP, Kvaratskhelia M, 2013 Structural basis for high-affinity binding of LEDGF PWWP to mononucleosomes. Nucleic Acids Res. 41, 3924–3936. [PubMed: 23396443]

Ferris AL, Wu X, Hughes CM, Stewart C, Smith SJ, Milne TA, Wang GG, Shun MC, Allis CD, Engelman A, Hughes SH, 2010 Lens epithelium-derived growth factor fusion proteins redirect HIV-1 DNA integration. Proc. Natl. Acad. Sci. U. S. A. 107, 3135–3140. [PubMed: 20133638]

Gijsbers R, Ronen K, Vets S, Malani N, De Rijck J, McNeely M, Bushman FD, Debyser Z, 2010 LEDGF hybrids efficiently retarget lentiviral integration into heterochromatin. Mol. Ther. 18, 552–560. [PubMed: 20195265]

Han BW, Wang W, Li C, Weng Z, Zamore PD, 2015 Noncoding RNA. piRNA-guided transposon cleavage initiates Zucchini-dependent, phased piRNA production. Science 348, 817–821. [PubMed: 25977554]

Handler D, Olivieri D, Novatchkova M, Gruber FS, Meixner K, Mechtler K, Stark A, Sachidanandam R, Brennecke J, 2011 A systematic analysis of Drosophila TUDOR domain-containing proteins identifies Vreteno and the Tdrd12 family as essential primary piRNA pathway factors. EMBO J. 30, 3977–3993. [PubMed: 21863019]

Jin Y, Wang Y, Walker DL, Dong H, Conley C, Johansen J, Johansen KM, 1999 JIL1: a novel chromosomal tandem kinase implicated in transcriptional regulation in Drosophila. Mol. Cell 4, 129–135. [PubMed: 10445035]

Klusza S, Deng WM, 2010 poly is required for nurse-cell chromosome dispersal and oocyte polarity in Drosophila. Fly (Austin) 4, 128–136. [PubMed: 20473032]

Kolasinska-Zwierz P, Down T, Latorre I, Liu T, Liu XS, Ahringer J, 2009 Differential chromatin marking of introns and expressed exons by H3K36me3. Nat. Genet. 41, 376–381. [PubMed: 19182803]

Li Y, Cai W, Wang C, Yao C, Bao X, Deng H, Girton J, Johansen J, Johansen KM, 2013 Domain requirements of the JIL-1 tandem kinase for histone H3 serine 10 phosphorylation and chromatin remodeling in vivo. J. Biol. Chem. 288, 19441–19449. [PubMed: 23723094]

Llano M, Vanegas M, Hutchins N, Thompson D, Delgado S, Poeschla EM, 2006 Identification and characterization of the chromatin-binding domains of the HIV-1 integrase interactor LEDGF/p75. J. Mol. Biol. 360, 760–773. [PubMed: 16793062]

Mereau H, De Rijck J, Cermakova K, Kutz A, Juge S, Demeulemeester J, Gijsbers R, Christ F, Debyser Z, Schwaller J, 2013 Impairing MLL-fusion gene-mediated transformation by dissecting critical interactions with the lens epithelium-derived growth factor (LEDGF/p75). Leukemia 27, 1245–1253. [PubMed: 23318960]

Qin S, Min J, 2014 Structure and function of the nucleosome-binding PWWP domain. Trends Biochem. Sci. 39, 536–547. [PubMed: 25277115]

Reeves R, Nissen MS, 1990 The A.T-DNA-binding domain of mammalian high mobility group I chromosomal proteins. A novel peptide motif for recognizing DNA structure. J. Biol. Chem. 265, 8573–8582. [PubMed: 1692833]

Regnard C, Straub T, Mitterweger A, Dahlsveen IK, Fabian V, Becker PB, 2011 Global analysis of the relationship between JIL-1 kinase and transcription. PLoS Genet. 7, e1001327.

Reyskens KM, Arthur JS, 2016 Emerging Roles of the Mitogen and Stress Activated Kinases MSK1 and MSK2. Front. Cell Dev. Biol. 4, 56. [PubMed: 27376065]

Shun MC, Botbol Y, Li X, Di Nunzio F, Daigle JE, Yan N, Lieberman J, Lavigne M, Engelman A, 2008 Identification and characterization of PWWP domain residues critical for LEDGF/p75 chromatin binding and human immunodeficiency virus type 1 infectivity. J. Virol. 82, 11555–11567. [PubMed: 18799576]

Staeva-Vieira E, Yoo S, Lehmann R, 2003 An essential role of DmRad51/SpnA in DNA repair and meiotic checkpoint control. EMBO J. 22, 5863–5874. [PubMed: 14592983]

Sutherland HG, Newton K, Brownstein DG, Holmes MC, Kress C, Semple CA, Bickmore WA, 2006 Disruption of Ledgf/Psip1 results in perinatal mortality and homeotic skeletal transformations. Mol. Cell Biol. 26, 7201–7210. [PubMed: 16980622]

Tesina P, Cermakova K, Horejsi M, Prochazkova K, Fabry M, Sharma S, Christ F, Demeulemeester J, Debyser Z, Rijck J, Veverka V, Rezacova P, 2015 Multiple cellular proteins interact with

LEDGF/p75 through a conserved unstructured consensus motif. Nat. Commun. 6, 7968. [PubMed: 26245978]

Turlure F, Maertens G, Rahman S, Cherepanov P, Engelman A, 2006 A tripartite DNA-binding element, comprised of the nuclear localization signal and two AT-hook motifs, mediates the association of LEDGF/p75 with chromatin in vivo. Nucleic Acids Res. 34, 1653–1665.

Vanegas M, Llano M, Delgado S, Thompson D, Peretz M, Poeschla E, 2005 Identification of the LEDGF/p75 HIV-1 integrase-interaction domain and NLS reveals NLS-independent chromatin tethering. J. Cell Sci. 118, 1733–1743. [PubMed: 15797927]

Wang CI, Alekseyenko AA, LeRoy G, Elia AE, Gorchakov AA, Britton LM, Elledge SJ, Kharchenko PV, Garcia BA, Kuroda MI, 2013 Chromatin proteins captured by ChIP-mass spectrometry are linked to dosage compensation in Drosophila. Nat. Struct. Mol. Biol. 20, 202–209. [PubMed: 23295261]

Wang Y, Zhang W, Jin Y, Johansen J, Johansen KM, 2001 The JIL-1 tandem kinase mediates histone H3 phosphorylation and is required for maintenance of chromatin structure in Drosophila. Cell 105, 433–443. [PubMed: 11371341]

Wiersma M, Bussiere M, Halsall JA, Turan N, Slany R, Turner BM, Nightingale KP, 2016 Protein kinase Msk1 physically and functionally interacts with the KMT2A/MLL1 methyltransferase complex and contributes to the regulation of multiple target genes. Epigenetics Chromatin 9, 52. [PubMed: 27895715]

Yasuhara JC, Wakimoto BT, 2008 Molecular landscape of modified histones in Drosophila heterochromatic genes and euchromatin-heterochromatin transition zones. PLoS Genet. 4, e16.

Yokoyama A, Cleary ML, 2008 Menin critically links MLL proteins with LEDGF on cancer-associated target genes. Cancer Cell 14, 36–46. [PubMed: 18598942]

Zhang L, Kasif S, Cantor CR, Broude NE, 2004 GC/AT-content spikes as genomic punctuation marks. Proc. Natl. Acad. Sci. U. S. A. 101, 16855–16860. [PubMed: 15548610]

Zhang W, Deng H, Bao X, Lerach S, Girton J, Johansen J, Johansen KM, 2006 The JIL-1 histone H3S10 kinase regulates dimethyl H3K9 modifications and heterochromatic spreading in Drosophila. Development 133, 229–235. [PubMed: 16339185]

Zhang W, Jin Y, Ji Y, Girton J, Johansen J, Johansen KM, 2003 Genetic and phenotypic analysis of alleles of the Drosophila chromosomal JIL-1 kinase reveals a functional requirement at multiple developmental stages. Genetics 165, 1341–1354. [PubMed: 14668387]

Zhang Z, Theurkauf WE, Weng Z, Zamore PD, 2012 Strand-specific libraries for high throughput RNA sequencing (RNA-Seq) prepared without poly(A) selection. Silence 3, 9. [PubMed: 23273270]

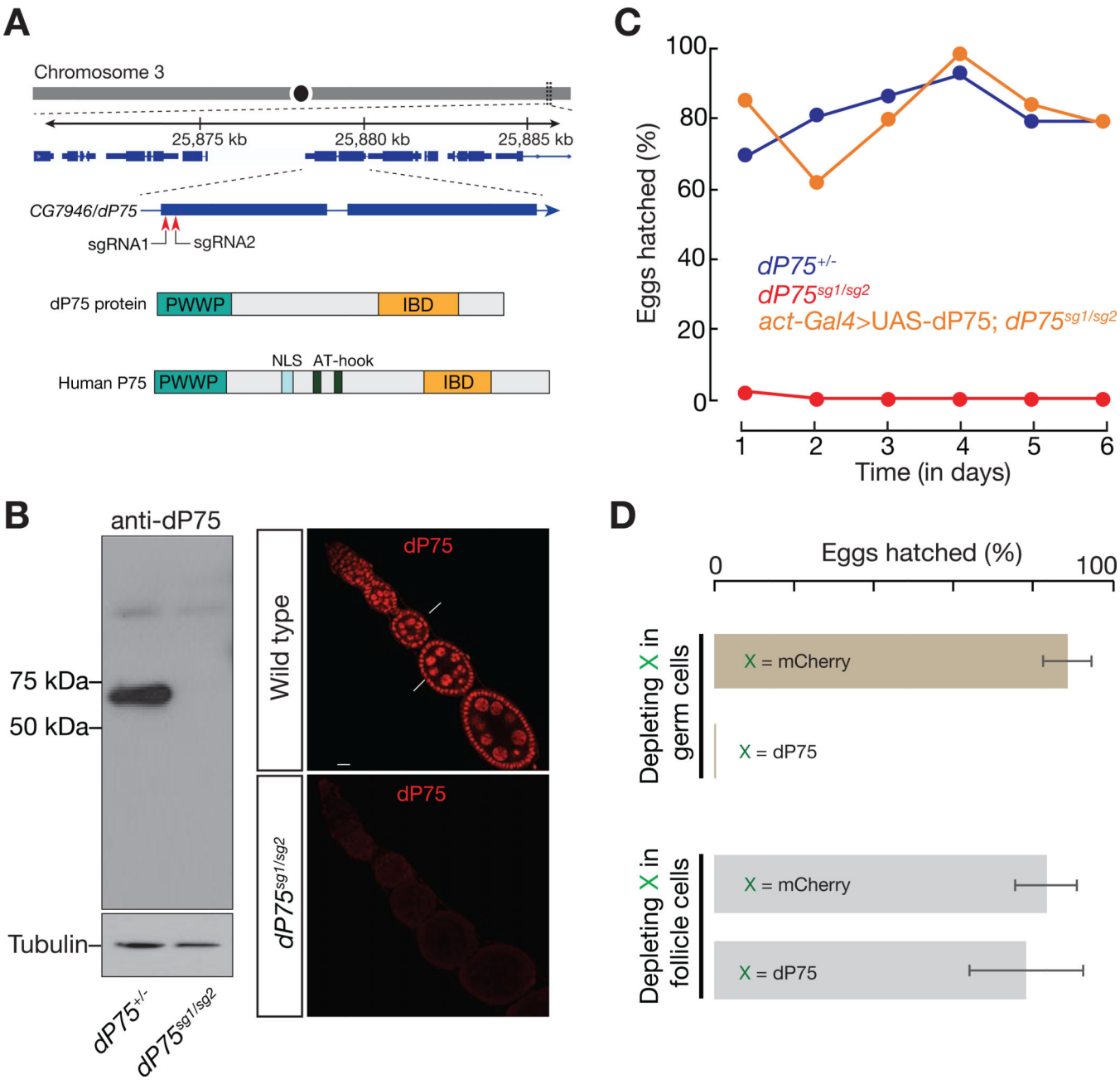

Fig. 1.

CG7946/dP75, the LEDGF/p75 homolog in Drosophila, is essential for female fertility. **A**: dP75 resides on the right arm of chromosome 3, encoding a protein with PWWP and LEGDF domains. IBD = Integrase-binding domain. Two sgRNAs used to generate *dP75* mutants are labelled. **B**: Characterization of *dP75* mutants. Left panel: western blot of ovarian lysate using polyclonal antibody against dP75. The bright band between 50kD and 75kD corresponds to the predicted size of dP75 protein. Right panel: immunostaining with dP75 antibody in wild-type and *dP75* mutant ovaries. **C**: Fertility of females over time. X-axis shows time (in days) since the hatch ratio experiment starts. Reintroducing dP75 transgene driven by actin-Gal4 into *dP75* mutant rescued the sterility phenotype. **D**: Fertility

of females with dP75 depletion in either germ cells or in somatic follicle cells. shRNA against mCherry was used as a control. The hatch ratio was counted as the average hatch ratio during the 6 days of egg-hatching experiment, and error bars = standard deviation.

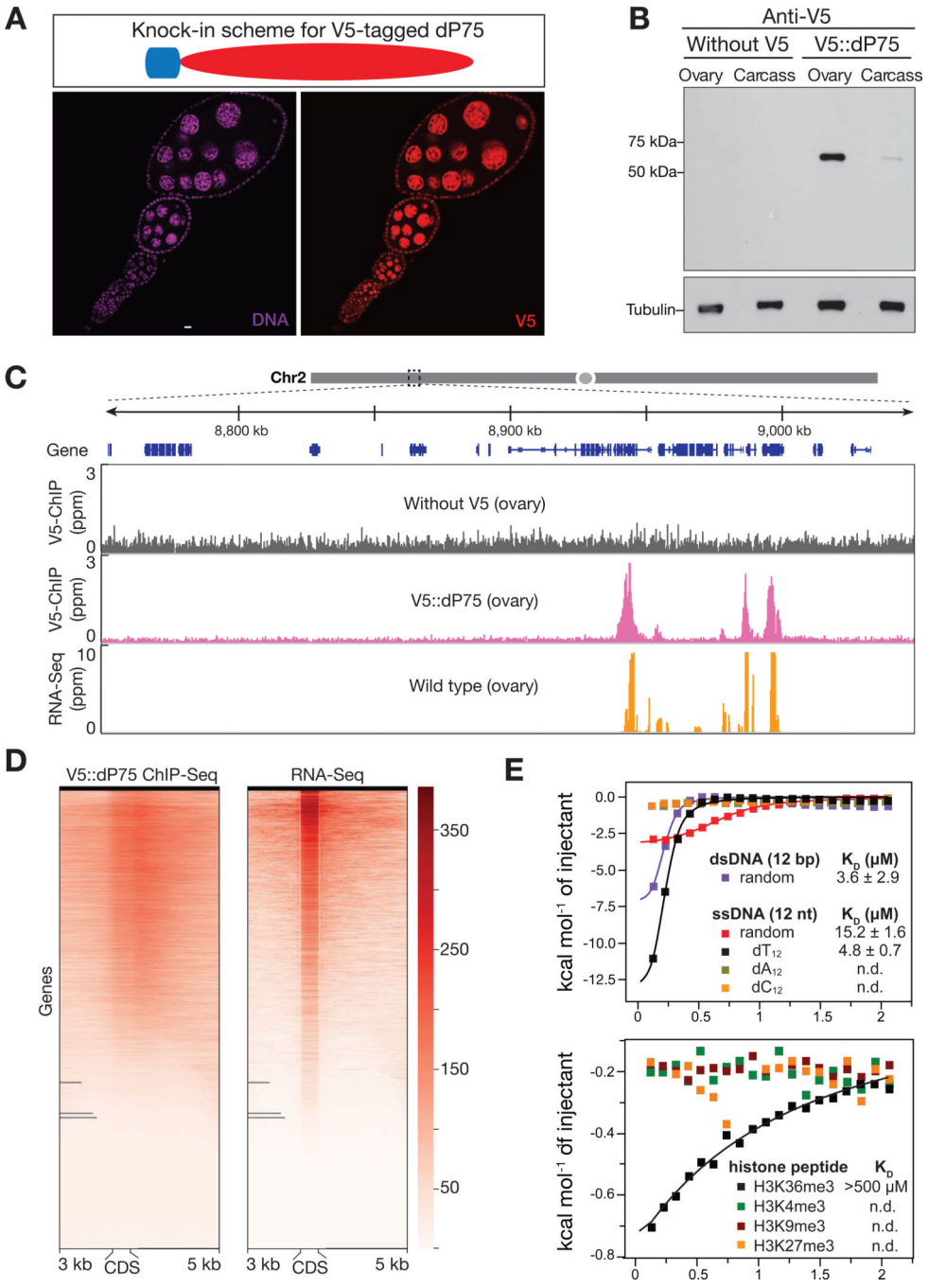

Fig. 2.

dP75 binds to actively transcribed chromatin regions *in vivo*. **A**: dP75 expression pattern as examined by V5 antibody staining in ovaries with V5 knocked-in at endogenous locus of dP75. **B**: Validation of V5 tag knock-in at endogenous dP75 locus by western blot. Western Blot were carried out using anti-V5 antibody. After V5 detection, the same membrane was used for western blot of internal control (using anti-Tubulin antibody). Carcass: fly body with ovaries ectomised. **C**: V5 ChIP-Seq and RNA-Seq signal across a 300 kb representative genome region on chromosome 2. V5 ChIP-seq performed in ovaries without V5 tag serves

as negative control. **D**: Heatmap for V5-dP75 ChIP-seq signal on genes and their mRNA levels in wild-type fly ovaries. Each line from the heatmap represents the coding region of one gene plus 3kb upstream and 5kb downstream of the coding region. **E**: Isothermal titration calorimetry (ITC) measurement of the binding affinity of PWWP domain to different oligos (upper panel), and various histone peptides (lower panel). ITC measurements were performed in duplicates. Binding isotherms and standard deviation were derived from nonlinear fitting using Origin 8.0 (MicroCal, Inc). The initial data point was routinely deleted. The ITC data were fit to a one-site binding model in 1:1 binding mode.

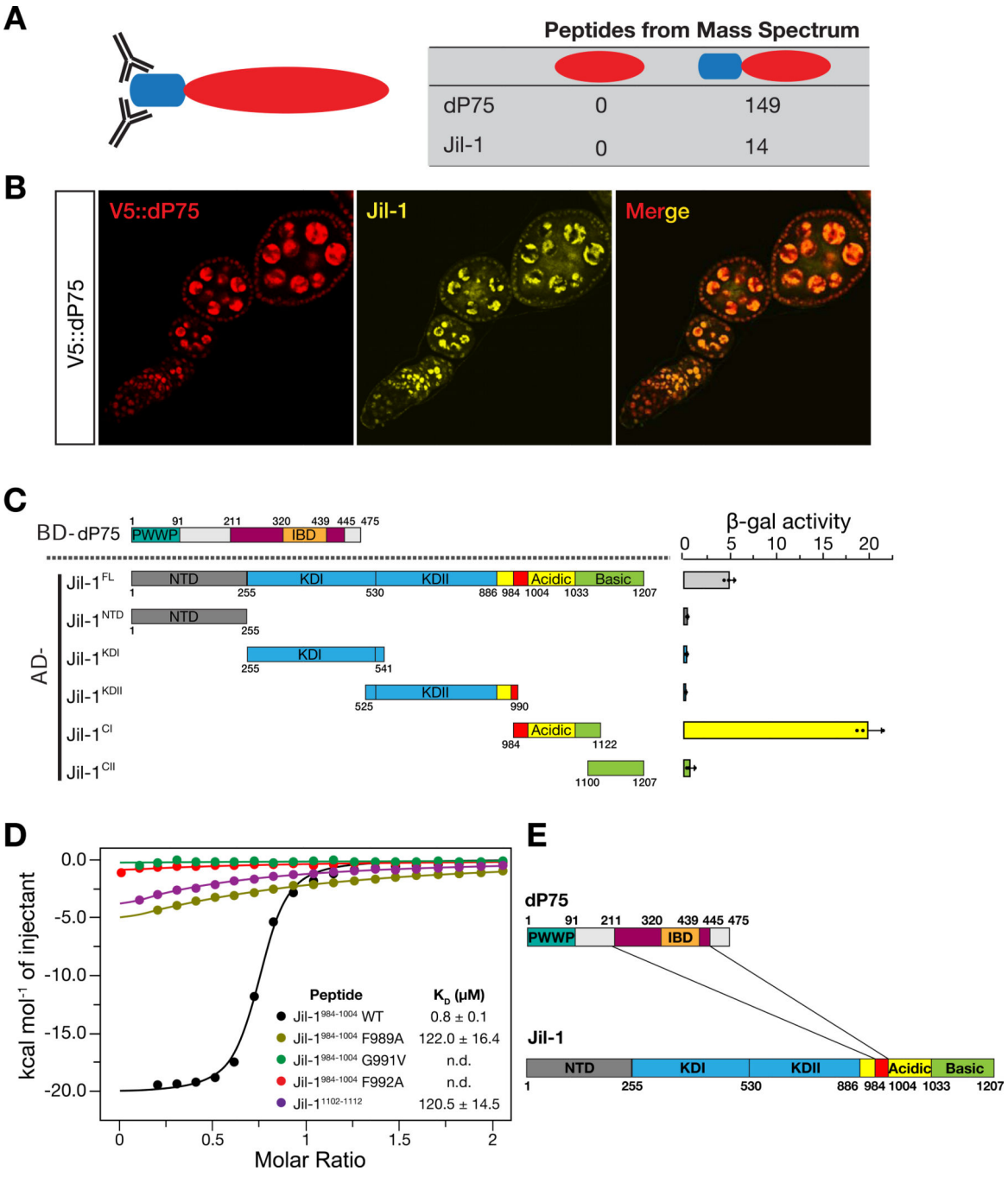

Fig. 3.

dP75 interacts with Jil-1 both *in vivo* and *in vitro*. **A**: Identification of dP75 interacting proteins by affinity purification and mass spectrometric analysis. The number of peptides identified from mass spectrometry for dP75 and Jil-1 in each sample is listed. **B**: dP75 and Jil-1 colocalize in fly ovaries. Immunostaining of fly ovaries were carried out using both V5 antibody (mouse) and Jil-1 antibody (chicken). At least two replicates were performed and reached the same results. **C**: Interaction measurement between dP75 and full-length or truncated versions of Jil-1 by yeast-two-hybrid assay. Interaction strengths are indicated by

β-gal activity. At least three independent clones were selected. Jil-1C1 fragment exhibits the strongest interaction with full length dP75. **D**: Isothermal titration calorimetry (ITC) to measure the interaction between dP75 and wild-type or mutated Jil-1 peptide (984–1004 fragment). Mutation of the conserved amino acids in the FYGF region of Jil-1 peptide severely attenuates its binding affinity with dP75. **E**: Graphic illustration for the interacting regions between dP75 and Jil-1.

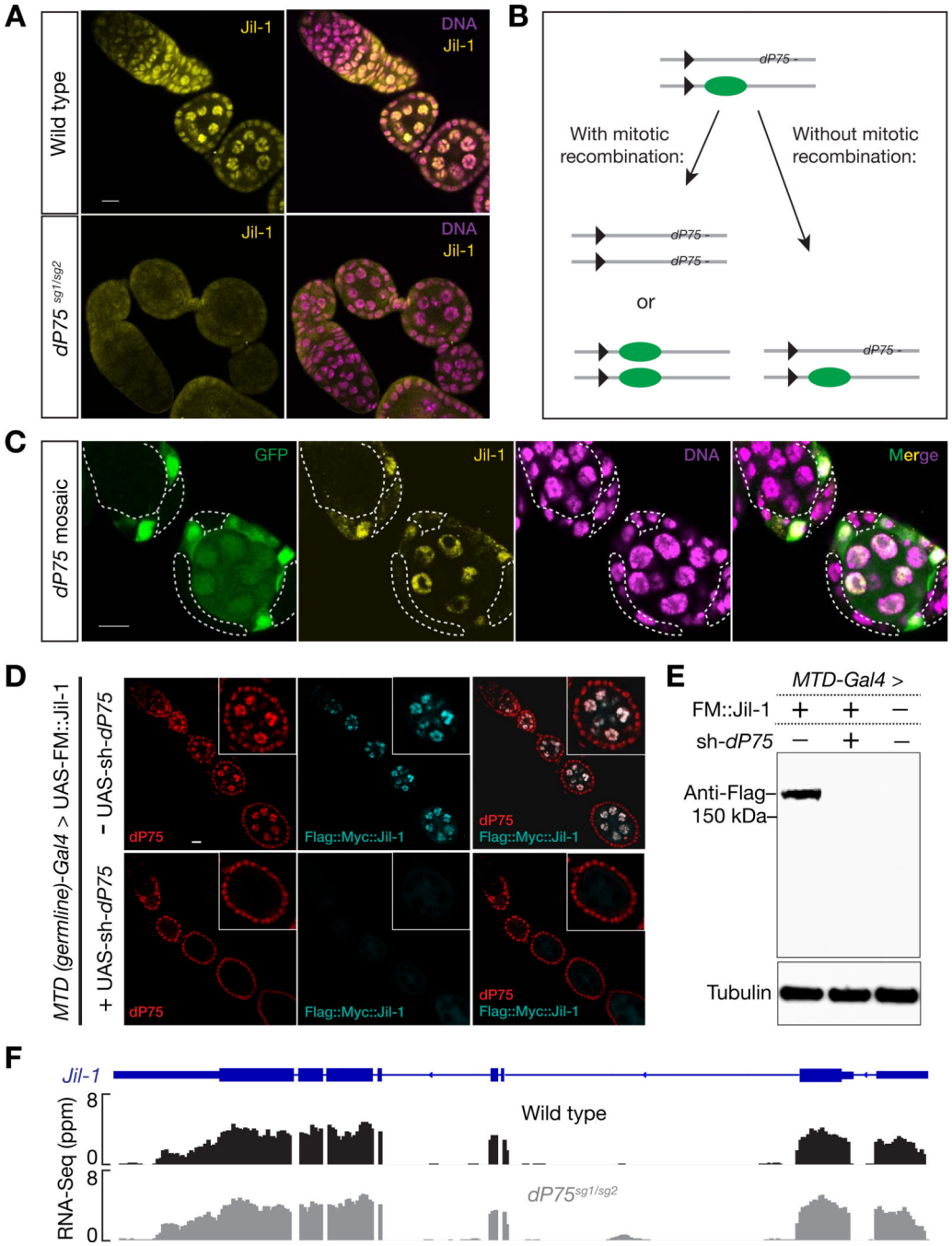

Fig. 4.

dP75 is required for stabilizing Jil-1 protein. **A**: Immunostaining of Jil-1 in the ovary from either wild-type or *dP75* mutants. Jil-1 shows robust nucleus-localized signal in wild-type flies, while these signals are nearly absent in *dP75* mutant. **B**: Strategy for mosaic analysis in (C). **C**: clonal analysis of Jil-1 expression. *dP75* mutant clones were generated through strategy shown in (B) and were subjected to immunostaining with Jil-1 antibody seven days after clone induction. *dP75* mutant clones are marked by absence of GFP, and outlined with dashed lines. The detailed method for clone generation is included in Method. **D**:

Immunostaining of transgenic Jil-1 protein in either control or in ovaries with dP75 depleted in germ cells. UAS-Flag::Myc::Jil-1 driven by germline specific Gal4 shows robust expression in wild type ovaries, but is undetectable when dP75 is depleted. **E**: Western blot for transgenic Jil-1 protein in control and dP75 depleted ovaries. **F**: RNA-Seq data show that the abundance of jil-1 mRNAs is not affected in *dP75* mutants.

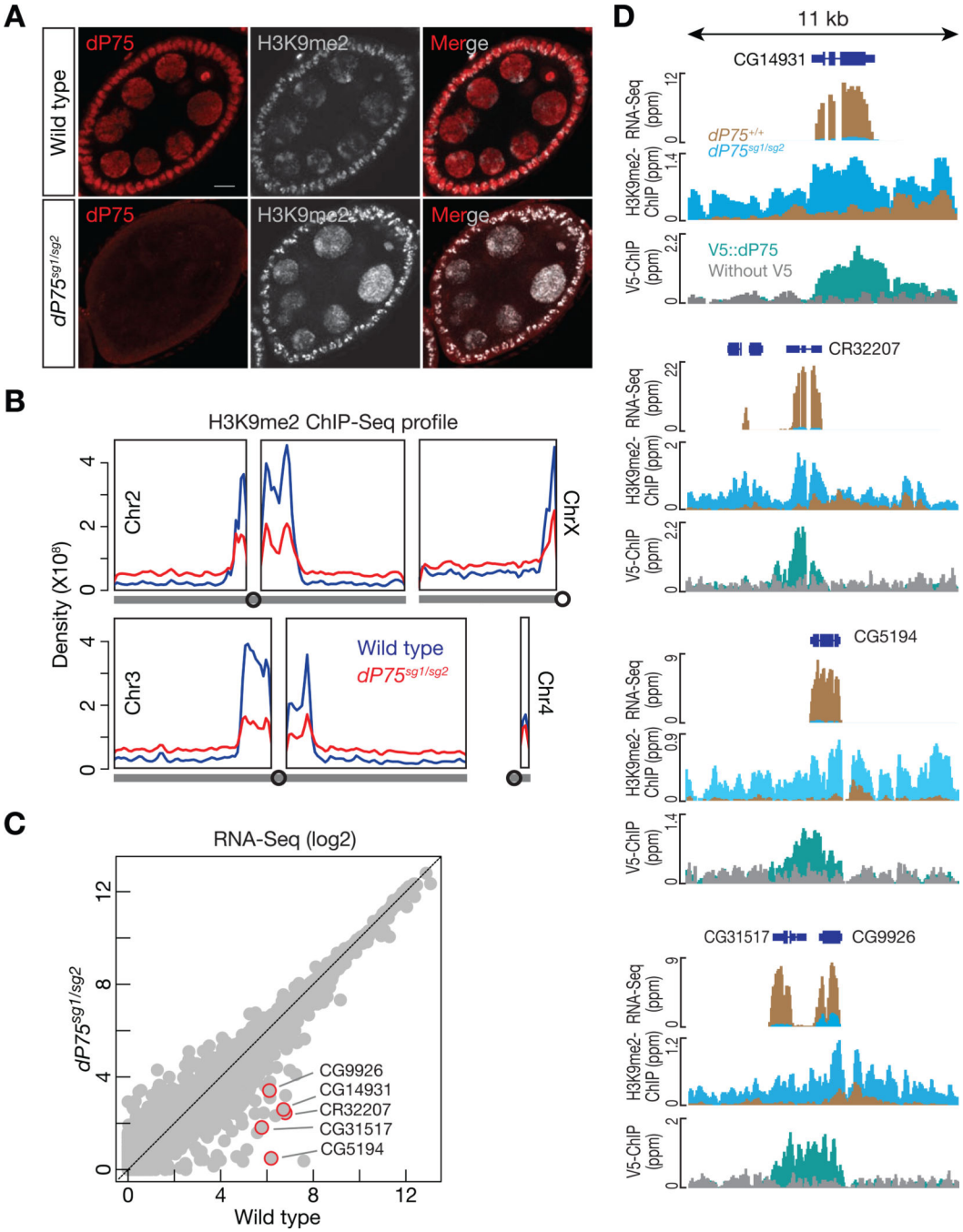

Fig. 5.

dP75 restrains H3K9me2 from spreading on chromosome arms. **A**: Co-immunostaining of dP75 and H3K9me2 in wild-type or *dP75* mutant ovaries. Three replicates were carried out and consistent patterns were observed in stage 6 to stage 8 egg chambers in each genotype. Representative pictures are shown here. **B**: Density of H3K9me2 ChIP-Seq signal across chromosome arms in wild-type or *dP75* mutant ovaries. The same sequencing depth (mapped reads) was used for analysis of the two samples, and the density of H3K9me2 ChIP-seq reads was calculated with Rstudio. **C**: Expression of genes measured by RNA-Seq.

Gene expression is calculated as FPKM, and both the x-axis and y-axis are in log2 scale. **D**: Browser view of RNA-Seq, H3K9me2 occupancy, and dP75 ChIP-seq signals for the top decreased genes in *dP75* mutants. Loss of dP75 leads to increase of H3K9me2 deposition and gene silencing.

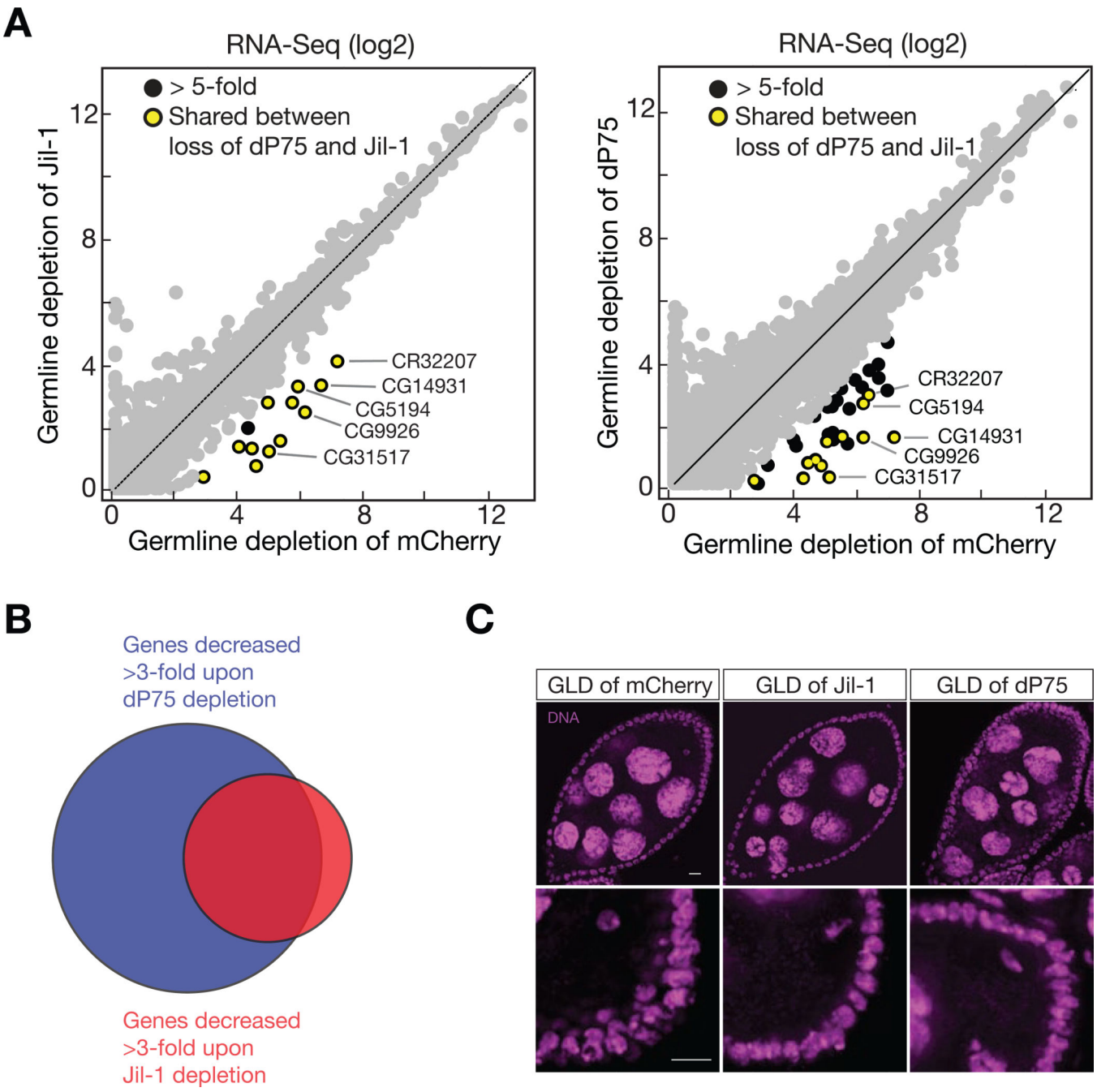

Fig. 6.

dP75 and Jil-1 function together to ensure oogenesis. **A**: Expression of genes measured by RNA-Seq. Gene expression is calculated as FPKM, and both the x-axis and y-axis are in log2 scale. **B**: dP75 and Jil-1 protect common targets for transcription. **C**: DAPI staining shows similar defects of germ cells by either depleting of dP75 or Jil-1 in germ cells. Upper panel: arrow heads point the nurse cells failed to pass the five-blob configuration. Percentage of each panel: 100% in GLD of mCherry (normal morphology); 57% in GLD of Jil-1 (abnormal morphology); 71% in GLD of dP75 (abnormal morphology). Stage 7 to stage 9 egg chambers were observed for quantification. Lower panel: oocyte DNA failed to compact

into karyosome (pointed by arrow head). Percentage of each panel: 98% in GLD of mCherry (normal morphology), 34% in GLD of Jil-1 (abnormal morphology), 27% in GLD of dP75 (abnormal morphology). Stage 7 to stage 8 egg chambers were observed for quantification.

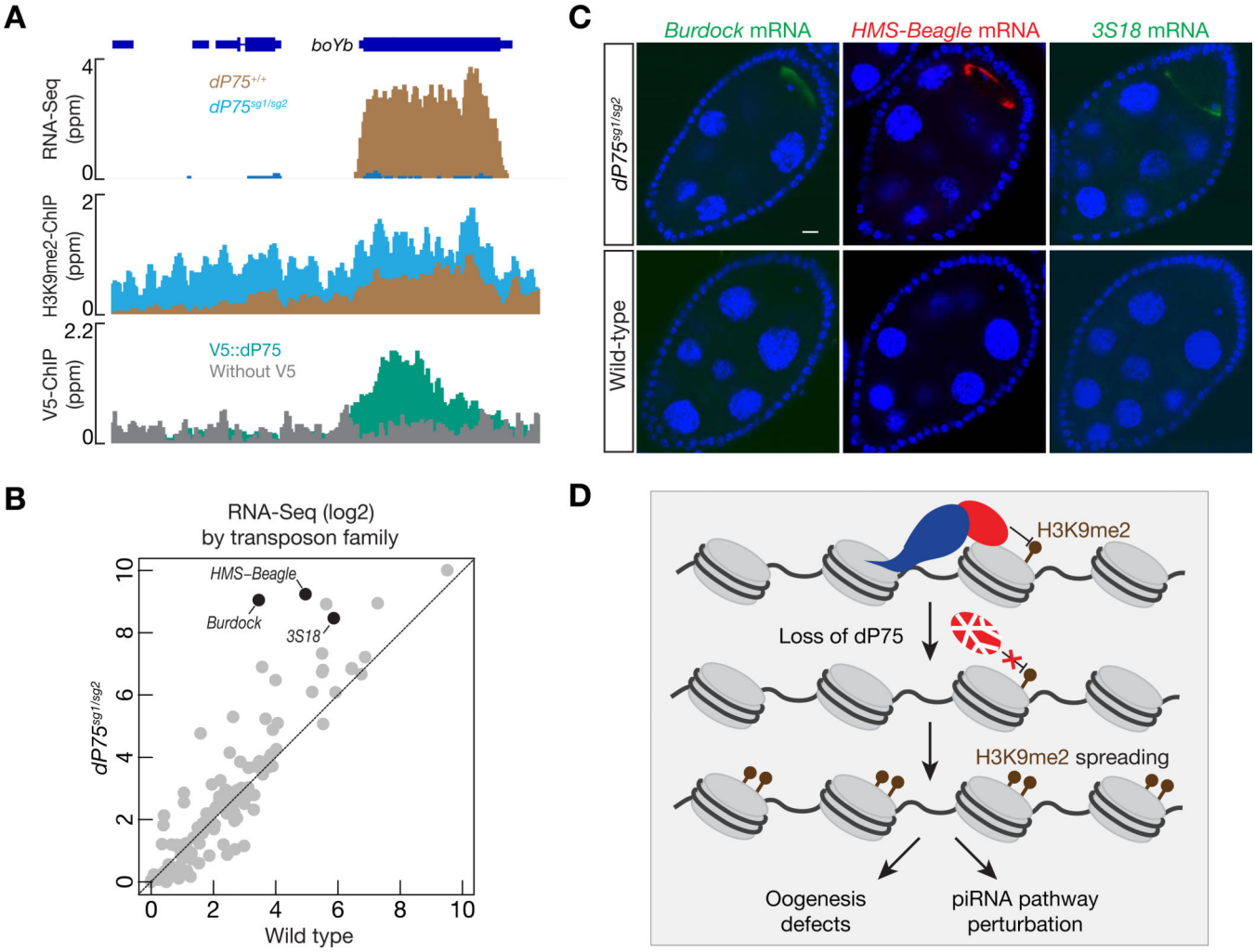

Fig. 7.

dP75 is required for transposon silencing during oogenesis. **A**: RNA-Seq, V5::dP75 ChIP-Seq, and H3K9me2 ChIP-Seq signals across the *boYb* gene, which encodes a piRNA pathway component for transposon silencing. dP75 protects *boYb* from H3K9me2 spreading. **B**: The change in transposon expression, relative to control, was compared for *dP75* mutants. Transposon expression is calculated as FPKM, and both the x-axis and y-axis are in log2 scale. **C**: RNA FISH to detect the expression and localization of transposon transcripts. **D**: Graphic model to depict the function of dP75 during oogenesis. dP75 physically interacts with Jil-1, antagonizing the spreading of H3K9me2. Upon loss of dP75, Jil-1 protein is unstable, and leads to H3K9me2 deposition on genes that are required for ensuring oogenesis and transposon silencing.

4.1. Table 1.

Reagents used in this study

REAGENT or RESOURCE	SOURCE	IDENTIFIER
Antibodies		
Anti-V5 tag mouse monoclonal antibody	Thermo Fisher Scientific, USA	CAT#: R960-25
Anti-V5 tag antibody (agarose)	Abcam, USA	CAT#: Ab1229
Rabbit polyclonal anti-dP75	This study	N/A
Chicken anti-Jil-1	Johansen lab	N/A
Mouse monoclonal anti-H3K9me2-ChIP grade	Abcam	CAT#: Ab1220
Mouse monoclonal anti-Flag M2 antibody	Sigma chemical, USA	CAT#: F3165-.2MG
Anti-alpha-tubulin antibody	DSHB, USA	12G10
Alexa 488 Donkey anti-Mouse	Thermo Fisher Scientific	CAT#: A-21202
Alexa 568 Goat anti-Mouse	Thermo Fisher Scientific	CAT#: A-11004
Alexa 488 Goat anti-Chicken	Thermo Fisher Scientific	CAT#: A-11039
Alexa 568 Goat anti-Rabbit	Thermo Fisher Scientific	CAT#: A-11011
Amersham ECL Mouse IgG, HRP-linked whole Ab	GE Healthcare Life Science, USA	NXA931-1ML
Amersham ECL Rabbit IgG, HRP-linked whole Ab	GE Healthcare Life Science	NA934-1ML
Experimental Models: Organisms/Strains		
D.melanogaster: w; Act5c-Gal4/CyO	Zhao Zhang lab	N/A
D.melanogaster: P(otu-Gal4::VP16.R)1 w[*]; P(Gal4-nos.NGT)40; P(Gal4::VP16nos.UTR)CG6325[MVD1]	Bloomington *Drosophila* Stock Center, USA	CAT#: 31777
D.melanogaster: *jil-1*-sh (attP2)	Bloomington *Drosophila* Stock Center	57293
D.melanogaster: *mcherry*-sh (attP2)	Bloomington *Drosophila* Stock Center	35785
D.melanogaster: *dP75*-sh (attP40)	Bloomington *Drosophila* Stock Center	55274
D.melanogaster: V5::dP75 (at its endogenous locus)	This study	N/A
D.melanogaster: UASP-FlagMyc-dP75 (attP40)	This study	N/A
D.melanogaster: UASP-FlagMyc-Jil-1 (attP2)	This study	N/A
D.melanogaster: *dP75-sg1/TM6c, sb*	This study	N/A
D.melanogaster: *dP75-sg2/TM6c, sb*	This study	N/A
Competent cells		
Top10 one shot kit	Life Technologies, USA	C404006
BL21 (DE3)	NEB, USA	C2527H
Critical Commercial Assay		
Vectashield Mounting Medium	VECTOR LABORATORIES INC MS	CAT#: 101098-042
V5 peptide	abcam	Ab15829
EDTA free complete protease inhibitor	Roche, USA	CAT#: 4693159001
pENTR™/D-TOPO® Cloning Kit	Thermo Fisher Scientific	K240020
Gateway™ LR Clonase™ II Enzyme mix	Thermo Fisher Scientific	11791020

REAGENT or RESOURCE	SOURCE	IDENTIFIER
Deposited Data		
Illumina Sequencing raw data (FASTQ)	This study	
Oligonucleotides		
Forward primer to validate V5 knockin: ACC CTC TTC TTG GTC TAG ATA	This study	N/A
Reverse primer to validate V5 knockin: AGC ATC TCG TTC CGG ATG TT	This study	N/A
Forward primer to sequence V5 knockin fly: ATA CGA GCA CTG CTA GCG C	This study	N/A
Forward primer to validate *dP75* knockout: ACC AAA CGA GCT AGA AGT CAA	This study	N/A
Reverse primer to validate *dP75* knockout: ATC GAT GGC CTC GAT GAA CT	This study	N/A
Forward primer to generate *dP75* transgene: CAC CAT GGG TAA GGA AAA GGC GGC	This study	N/A
Reverse primer to generate *dP75* transgene: TTA CTG TGG AGC CGA TCC G	This study	N/A
Forward primer to generate jil-1 transgene: CAC CAT GAG TCG CTT GCA AAA GCA A	This study	N/A
Reverse primer to generate jil-1 transgene: TCA TTG GAA CTG ATA AAG TTG AC	This study	N/A
Software and Algorithms		
piPipes	Han et al. (2015)	N/A